HHS Public Access

Author manuscript

New J Phys. Author manuscript; available in PMC 2016 June 01.

Published in final edited form as:

New J Phys. 2015 June ; 17(6): . doi:10.1088/1367-2630/17/6/063013.

Anomalous segregation dynamics of self-propelled particles

Enys Mones[1,*], **András Czirók**[1,2,†], and **Tamás Vicsek**[1,3,‡]

[1]Department of Biological Physics, Eötvös Loránd University, Pázmány Péter stny. 1/A, H-1117 Budapest, Hungary

[2]Department of Anatomy & Cell Biology, University of Kansas Medical center, Kansas City, KS, USA

[3]Biological Physics Research Group of HAS, Pázmány Péter stny. 1/A, H-1117 Budapest, Hungary

Abstract

A number of novel experimental and theoretical results have recently been obtained on active soft matter, demonstrating the various interesting universal and anomalous features of this kind of driven systems. Here we consider the adhesion difference-driven segregation of actively moving units, a fundamental but still poorly explored aspect of collective motility. In particular, we propose a model in which particles have a tendency to adhere through a mechanism which makes them both stay in touch and synchronize their direction of motion – but the interaction is limited to particles of the same kind. The calculations corresponding to the related differential equations can be made in parallel, thus a powerful GPU card allows large scale simulations. We find that in a very large system of particles, interacting without explicit alignment rule, three basic segregation regimes seem to exist as a function of time: i) at the beginning the time dependence of the correlation length is analogous to that predicted by the Cahn-Hillard theory, ii) next rapid segregation occurs characterized with a separation of the different kinds of units being faster than any previously suggested speed, finally, iii) the growth of the characteristic sizes in the system slows down due to a new regime in which self-confined, rotating, splitting and re-joining clusters appear. Our results can explain recent observations of segregating tissue cells *in vitro*.

Keywords

spp model; cell segregation; nonequilibrium; dynamical exponents

I. INTRODUCTION

Collective flow of self-propelled biological units is observed on many scales ranging from molecular motor-driven cytoskeletal polymers, microscopic organisms, tissue cells and animals [1]. Non-living objects under specially designed conditions, such as fluidized

*Electronic address: enys@hal.elte.hu
†Electronic address: andras@biol-phys.elte.hu
‡Electronic address: vicsek@hal.elte.hu

PACS numbers: 87.17.-d, 87.15.Zg, 05.65.+b

granular materials [2], surface tension difference-driven “Janus particles” [3, 4], light pushed colloids [5] or micron-sized edges [6] or spheres rotating due to an applied electric field [7] can also behave as self-propelled particles. All these systems, active fluids, exhibit unusual behavior like the emergence of long-range correlations, superdiffusive behavior, anomalous density fluctuations, or explosive aggregation dynamics [8].

Here we focus on the unusual segregation dynamics of a mixture of different kinds of self-propelled particles at high density surface coverage. Segregation may occur due to the difference in the motilities of the particles [9, 10] but in inanimate systems it is typically driven by adhesion differences, like the preferred adhesion to objects of the same type, and manifests as a slow coarsening described by the Cahn-Hilliard equation [11]. In binary mixtures the characteristic domain size λ grows in time, t, as

$$\lambda \sim t^{z} \quad (1)$$

with $z = 1/3$ for even coverage ratios, and $z = 1/4$ for unequal coverage rations [12]. These exponents reflect a dynamics in which particles move only by diffusion, thus there are no convective currents present. For even coverage ratios the two kinds of particles segregate into a labyrinth pattern, while distinct clusters (islands) emerge at uneven coverage ratios. Both the labyrinth and island patterns coarsens by merger of adjacent structures and the subsequent interface minimization driven by surface tension. Yet, this dynamics is expected to change when the particles have an intrinsic motility, which is not driven by a free energy gradient of the whole system. For example, ballistically moving clusters are expected to aggregate faster [13]. Yet the presence of slower moving objects, and the corresponding excluded volume constraints can make this process different from the aggregation of self-propelled clusters from a low density phase. In addition, the slower objects may also organize into a confinement barrier, strongly influencing the flow of more active particles [9].

Such segregation settings are also achievable in most experiments using non-living self-propelled objects. The interaction between highly active and more stationary (but not necessarily less adhesive) units is also relevant in crowd control [14], but perhaps most obviously in multicellular systems. Cells of the same type segregate into disjunct clusters during various stages of embryonic development, often utilizing both adhesion and motility differences [15].

To explain this phenomenon, the differential adhesion hypothesis (DAH) [16] proposed that cell types have distinct adhesion properties. However, while the DAH and the corresponding computational models yield a slow coarsening similar to Cahn-Hilliard exponents [12], recent experiments revealed a much faster segregation dynamics, with

$$1/2 < z < 1 \quad (2)$$

for both in 3D spheroid [17] and 2D monolayer [18] cultures. This increased coarsening exponent is likely to contribute to the surprisingly fast development of early embryos.

Anomalous sorting was reported within a self-propelled particle system in which particles actively align their motion directions and interact with a hard core short range repulsion and a somewhat longer, but still short range attraction [20]. This pioneering study indicated, for the first time, that taking into account the self-propelled nature of the units leads to qualitatively new behavior as compared to simple diffusion-like motion. While the exponent z was not determined directly, an analogous measure indicates $z \sim 0.18 < 1/3$ as discussed in [12]. Here we demonstrate that the self-propelled nature of the units (i.e., active cell motility) can substantially speed up the Cahn-Hilliard segregation dynamics and can yield behavior compatible with the experimentally observed z values in 2D cell cultures (2). Following [21], we define a self-propelled particle model of binary mixtures. In the considered model particles interact with short range inter-particle forces and also adjust the direction of self-propulsion in response to these forces. By large scale computer simulations we explore the segregation dynamics and the spontaneously developing velocity fields. Our simulations indicate that in a very large system of particles, interacting without an explicit alignment rule, three basic segregation regimes seem to exist as a function of time: i) at the beginning the time dependence of the correlation length is analogous to that predicted by the Cahn-Hillard theory, ii) next rapid segregation occurs characterized with a separation of the different kinds of units being faster than any previously suggested speed, finally, iii) the growth of the characteristic sizes in the system slows down due to a new regime in which self-confined, rotating, splitting and re-joining clusters appear.

II. THE SEGREGATION MODEL

Self-propelled particles (SPPs) are modeled using the following two-dimensional overdamped equation of motion:

$$\frac{\mathrm{d}\vec{r}_i}{\mathrm{d}t} = v_0 \vec{n}_i + \vec{F}_i, \quad (3)$$

where $\vec{r_i}$ is the position of the ith particle, v_0 and $\vec{n}$ are the magnitude and direction of its active motion and $\vec{F}$ denotes the (net) force acting on the particle resulted from short range interactions with its environment. Forces are exerted by other particles and the boundary, modeled as a repulsive rigid wall:

$$\vec{F}_i = \sum_{j=1}^{N} \vec{F}^{cell}(\vec{r}_i, \vec{r}_j) + \vec{F}^{wall}(\vec{r}_i). \quad (4)$$

Following [21], we model the interparticle force with a piecewise linear function of the distance $d_{ij} = |\vec{r_i} - \vec{r_j}|$. This force represents the combination of a shorter range repulsive and longer range adhesive interaction as

$$\vec{F}^{cell}(\vec{r}_i, \vec{r}_j) = \frac{\vec{r}_j - \vec{r}_i}{d_{ij}} \begin{cases} F_{rep}\frac{d_{ij}-a_{eq}}{a_{eq}}, & \text{if } d_{ij} < a_{eq}, \\ F_{adh}\frac{d_{ij}-a_{eq}}{R_0-a_{eq}}, & \text{if } a_{eq} < d_{ij} < R_0, \\ 0, & \text{otherwise.} \end{cases} \quad (5)$$

In expression (5) the interaction range is R_0, and a_{eq} denotes the equilibrium distance where the attractive and repulsive forces are balancing each other. In the simulations, R_0 and a_{eq} are set so that the cells behave as soft disks and the interaction range is slightly larger than their diameter. The coefficients F_{rep} and F_{adh} set the strength of the repulsion and adhesion, respectively. We assumed that adhesion is absent between cells of different types ($F_{adh}^{\mathscr{R}-\mathscr{G}}=0$), and the repulsion coefficient is fixed for all cell interactions.

The boundary exerts a force that is exponentially decreasing with the distance from the wall d_{iw}:

$$\overrightarrow{F}^{wall}(d_{iw})=\overrightarrow{e}_{iw}\begin{cases} F_w\exp\left(-\frac{2d_{iw}}{R_0}\right), & \text{if } d_{iw}<R_0, \\ 0, & \text{otherwise,} \end{cases} \quad (6)$$

where $e_{iw}^{\rightarrow}$ is the unit vector pointing to the closest boundary segment and the F_w coefficient sets the magnitude of this force.

Finally, SPP heading vectors are steered towards the particles' physical displacements by the rule proposed in [21]:

$$\frac{\mathrm{d}\theta_i}{\mathrm{d}t}=arg(\overrightarrow{v}_i)-\theta_i+\xi \quad (7)$$

where θ_i = arg(n_i)$^{\rightarrow}$ is the angle of heading vector $n_i^{\rightarrow}$ and arg(v_i)$^{\rightarrow}$ is the angle of the actual velocity as influenced by interparticle forces. This steering is, however, imperfect – which is modeled by a Gaussian white noise with zero mean and finite variance

$$\langle\xi(t)\xi(t')\rangle=\frac{\eta^2}{12}\delta(t,t'). \quad (8)$$

The motivation for such a steering rule comes from observations indicating that cells can respond to mechanical forces [23–27]. It is also consistent with a positive feedback regulation of front-rear cell polarity by actual cell displacements (actin polymerization in the front of the cell) [28] as discussed further in [29].

We compare the above defined SPP model with a similar conventional Brownian particle model in which particles move in completely random directions:

$$\overrightarrow{n}_i(t)=\overrightarrow{\xi}, \quad (9)$$

where the noise $\xi^{\rightarrow}$ is a two-dimensional random vector with zero mean and finite variance.

To demonstrate the importance of the steering rule (7), we also performed simulations with persistent Brownian particles, where Eq. 7 has been replaced by

$$\frac{\mathrm{d}\theta_i}{\mathrm{d}t}=\xi. \quad (10)$$

Throughout of this paper we use the notation “SPP” for particles obeying the steering rule (7), except one place (Fig. 2, Results section) where we make it explicit that self-propelled particles with the so called alignment rule (a particle is instntaneously taking on the evarage direction of its neighbours) segregate rather differently from the ones governed by the steering rule.

III. PARAMETERS

Simulations were carried out in a closed rectangular domain of size L with repulsive walls. We investigated the segregation of two different types of particles – being referred to below as red ($\mathcal{R}$) and green ($\mathcal{G}$). Model parameter values were assigned to particles depending on which group they belonged to. The choices of the parameter values for the two particle types were motivated by the observations of cell sorting in monolayers [18]. Thus, the red particles are larger, more motile and have stronger adhesive force among each other. We assumed that while short-range repulsion exists between each particle, the attractive force acts only between particles of the same type.

The number of particles was set to obtain a close to fully packed coverage of the entire simulation area (mostly in the range of 90% coverage). While the average particle “size” (a_{eq}) was determined by the particle type (a_{eq} = 1 for red and a_{eq} = 0.5 for green particles), the actual size of each particle was randomly selected from a uniform distribution between [a_{eq} − 0.1, a_{eq} + 0.1]. Thus both particle groups were polydisperse. In a polydisperse system the interaction (5) is evaluated using the average R_{eq} values of the interacting partners. The interaction range was set as $R_0 = 1.4a_{eq}$. The number of particles of a given type was determined from a target surface coverage. As an example, to achieve a 1:1 coverage ratio, the number of particles was inversely proportional to their size: $N_{\mathcal{R}}/N_{\mathcal{G}} = a_{\mathcal{G}}^2/a_{\mathcal{R}}^2$.

The natural length scale of the simulations is the mean diameter of a (red) particle, a_{eq} = 1. The natural time unit of the simulations, t, is the time that is needed for a cell to move a distance of the average diameter. Since this time depends on a number of model parameters, our time units are fixed as the natural time units of the simulations corresponding to the parameter values given in Table 1.

As reported previously [21], the main control parameter of the model is the precision of the steering term. When adaptation of the heading and movement vectors is precise (i.e., the noise in Eq. (7) is small), the system organizes into a long-range ordered state. In this state particle velocities are correlated over distances that are comparable with the system size. As the simulations are carried out in a finite domain with repulsive walls, in the long-range ordered regime the whole system rotates in a randomly selected direction. Since this state was not directly observed in cell sorting experiments, for our simulations we have chosen a parameter setting which does not lead to correlated motion within the entire simulation domain, yet the steering is precise enough to build velocity correlations over substantial distances.

IV. RESULTS

A. Dynamic exponents from simulations

We performed simulations of the segregation process. As an initial condition we chose a random binary mixture – a configuration in which particles do not overlap, but particle types are assigned randomly and independently. Such binary mixtures readily segregate into homogeneous clusters, both for even and uneven coverage ratios (Fig. 1). As the supplemental movies demonstrate, clusters of segregated particles are highly motile and may even reach a state where all particles segregate into a single, rotating cluster. Snapshots of cell cultures in Fig. 1 show the 2D segregation of EPC (green) and primary fish keratocytes (red) obtained from [18]. To derive the natural time unit τ for the experiments, we considered that the diameter of fish keratocytes is $a \approx 20\mu$m, and have a persistent velocity of $v_0 \approx 500\mu$m/h. Thus, the characteristic time – needed for a displacement the size of a unit cell diameter – in the experiment is $\tau \approx 2$min. When time is measured in the natural unit, the corresponding simulated and experimentally observed configurations are very similar.

The characteristic spatial scale λ of a given configuration was determined by wavelet transform [22]. Segmented images of the simulated system were convolved with a series of two-dimensional Mexican hat wavelets – each with a distinct scale parameter. The characteristic scale was set as the wavelet parameter that yields the largest standard deviation in the convolved image. Repeating this procedure for a series of configurations was used to characterize the time development of the segregation process. As Fig. 2 demonstrates for an even coverage of the two particle types, both the Brownian and the persistent random walker (10) systems exhibit the characteristic Cahn-Hilliard behavior with $z = 1/3$. In contrast, the segregation of the SPP simulation is triphasic. After an initial, Cahn-Hilliard-like behavior a fast segregating regime sets in with $z \approx 1$. In this regime the particles rapidly organize into giant clusters. Finally, sufficiently large simulations reach a new regime characterized by self-confined, rotating clusters that may split and re-join depending on their internal dynamics. While particles stream within these clusters, the whole system – composed of the two kinds of particles – do not exhibit long range-ordered movements.

The same behavior also emerges in simulations with much simpler parameter choices, when the segregation is driven only by the lack of adhesion between the red and green particles (Fig. 2 inset). The specific steering rule (7), however, is important to generate the reported behavior. For example, as Fig. 2 demonstrates, an analogous system does not segregate if the only difference is that steering rule is replaced by the velocity alignment rule of [30]. In that system the lack of local velocity variations can effectively inhibit the segregation process.

To investigate how model and simulation parameters affect the segregation of SPP mixtures guided by the steering rule (7), the system size, noise and the red-green coverage ratio was systematically varied from the parameter setup used to generate Figs 1–2. As Fig. 3A demonstrates, the segregation is faster and its onset is earlier when steering noise is decreased. The transition between the fast ($z \approx 1$) and slow ($z \approx 1/3$) regimes is sudden: it is elicited by a 10% change in the noise amplitude. The transition between coarsening regimes

is coincident with the transition between a long-range ordered (rotating, blue and orange symbols in Fig. 3A) and a locally ordered, but globally disordered system (yellow and green symbols in Fig. 3A). In a transient regime (red symbols in Fig. 3A) the velocity correlation length is still smaller than the system size, yet the segregation is much faster than the Cahn-Hilliard behavior.

Simulations performed with various system sizes (Fig. 3B) reveal an intrinsic (system size independent) upper limit for the linear cluster growth regime. For uneven coverage ratios the coarsening is slower both in the SPP (Fig. 3C) and the Cahn-Hilliard-type Brownian system (Fig. 3D). Still, coarsening in the the SPP system continues to be fast as the table of exponents indicate.

The results shown in Fig. 3 thus indicate that fast segregation is characteristic for the locally ordered, but globally disordered regime of the SPP system. As spatially correlated movements seem to be of key importance, in Fig. 4 we show velocity field snapshots that are representative for various stages of the segregation process. The parallel increase of the velocity correlation length and pattern size indicate that in the SPP model clusters can move coherently for extended distances. In contrast, a local diffusive movement is characteristic for the Cahn-Hilliard-type Brownian system. The velocity snapshots also reveal that clusters can readily glide along each other as motion directions can change abruptly at cluster boundaries (Fig. 4C).

B. Qualitative Interpretation

The different exponents in the Brownian and SPP system can be qualitatively understood if we compare the predominantly diffusive (Brownian) and SPP aggregation kinetics [19]. Let us consider the system at time t_1 when the characteristic size of the motile clusters is λ_1. By time t_2 the typical cluster size is increased to $\lambda_2 = \sqrt{2}\lambda_1$ reflecting the coalescence of two clusters of size λ_1. If the typical distance separating the clusters was λ_1' at time t_1, it is increased to λ_2' at time t_2. A typical pattern unit consists of a dense cluster of particles occupying an area of size λ^2, surrounded by an empty area of the size λ'. If the particle density within the clusters is constant then the number of particles is proportional to the size of the cluster, hence the average particle density is given by $\lambda^2/(\lambda + \lambda')^2$. Due to the conservation of particles, this quantity remains the same throughout the process yielding $\lambda_2' = \sqrt{2}\lambda_1'$. Hence, during the coarsening process we expect that both the size of the clusters and the distance separating the clusters increases by a similar factor, which yields $\lambda \sim \lambda'$.

First, let us focus on the segregation dynamics of Brownian particles. During a sufficiently small time interval Δt, each particle within a noise driven cluster is subjected to a random displacement, $v_0 \int_0^{\Delta t} \vec{\xi}(\tau) d\tau$ according to Eqs (3) and (9). For a cluster of $N \sim \lambda^2$ particles the vectorial sum of these displacements is a random vector with zero mean and standard deviation $v_0 \eta \sqrt{N \Delta t}$. If the attractive forces within the cluster are strong enough to maintain its integrity, the cluster's center of mass performs a random walk: the standard deviation of the center of mass displacement is $v_0 \eta \sqrt{\Delta t / N}$. After an elapsed time t (thus after $t/\Delta t$ steps)

the variance of the center of mass is $v_0^2\eta^2 t/N$. Hence, the cluster's diffusion coefficient depends on its size λ as

$$D(\lambda)=\frac{v_0^2\eta^2}{4N}\sim\lambda^{-2}. \quad (11)$$

The time expected to move the cluster over a distance $\lambda_1^{'}$ is

$$t_2-t_1\sim\frac{\lambda_1^{'2}}{D(\lambda_1)}\sim\lambda_1^4. \quad (12)$$

As $t_2-t_1\sim\lambda_1^{1/z}$, for the aggregation of Brownian clusters we obtain the Cahn-Hilliard result of $z = 1/4$.

In contrast, particles in the SPP model move superdiffusively as for their displacement d over time t

$$d\sim t^{\alpha} \quad (13)$$

holds with $a \approx 1$. Due to the extended spatial range of velocity correlations the cluster speed only weakly depends on cluster size. Thus

$$\lambda_1^{'}\sim(t_2-t_1)^{\alpha} \quad (14)$$

yielding $z = a$. For ordered SPP motion $a = 1$, in our simulations $a \approx 0.8$.

The above arguments assumed that the segregation process is driven by the merger of individual clusters. When the coverage ratio of the two particle types is 50:50, the system organizes into stripes instead of clusters. In the Brownian case the value of the dynamic exponent $z = 1/3$ corresponds to a situation in which the coarsening is driven by the lateral movement of the stripes performing a random walk with a diffusivity $D(\lambda) \sim \lambda^{-1}$.

V. DISCUSSION

Active motion within a confluent (densely packed) system is susceptible to jamming [31]. While the polydisperse particle size distribution helps to prevent the formation of a crystalline lattice, the formation of coherently moving clusters for low noise are similar to the "glider" structures that develop in high density lattice gas simulations [32]. An off lattice, overdamped SPP model with excluded volume interaction was recently shown to undergo spontaneous phase separation, by which particles create a dense cluster that is immersed in a "gas phase" of low particle density. Such a system, without the specific steering rule (7) linking propulsion direction to physical displacements, exhibits an aggregation kinetics with $z = 1/2$ [33]. Recent scaling analysis of the irreversible SPP coagulation process indicated the possibility for $z > 1$ and in certain cases even explosive

cluster growth where the cluster size increases exponentially in time [13]. While the high particle density and the reversible association of the particles prevents the realization of such explosive coarsening in our simulations, these recent result indicate that self-propelled systems can coarsen substantially faster than the Cahn-Hilliard behavior. In almost all cases the pattern we have observed could be characterized as a connected “mesh” of one type of the particles and the other type consisting of isolated clusters moving (sometimes rotating) within the boundaries defined by the mesh. We have found that the particles with smaller velocity and a smaller amount of persistence form the mesh-like boundary for the more motile other type.

A comparison of our results to that of [20] and [34] reveals that the actual steering mechanism of SPP systems is very important. This difference is partially captured by models operating with polar or apolar alignment rules: in the former particles tend to move in a parallel direction, while in the latter particles can readily glide in opposite directions, like self-propelled rods [35–37]. Here there is no explicit “polar” coupling between the velocity of adjacent particles, yet they readily organize into a polar order. Arguably, our steering rule (7) represents an indirect polar coupling being present as each particle tends to align with its own velocity which is determined by interactions with the neighbors. Yet, if we substitute the steering rule (7) with the velocity alignment rule of [30] no segregation occurs irrespectively of the noise within the system. The same velocity alignment rule, combined with a different equation of motion, allows a slow segregation of particles in [20]. Thus, the segregation behavior is rich and surprisingly dependent on certain model properties. In addition to the differences demonstrated in Fig. 2, the simplest, symmetrical choice of parameteres (same adhesion between red and green particles, same motility) segregate slowly due to jamming. In contrast, the same parameter settings can yield $z \approx 1$ when the coverage is slightly decreased (Fig. 2, inset). Thus, fast segregation depends on the emergence of fast moving clusters. When the persistent motion of clusters is hindered either by jamming, extensive mixing, or the lack of cohesion – the slower, diffusive Cahn-Hilliard behavior appears.

Embryonic morphogenesis and tissue regeneration are fascinating, complex processes. Cell sorting is one of the fundamental concepts that help us understand how multicellular patterns form at various stages of development. During cell sorting cells of the same type segregate into disjunct clusters. To explain this phenomenon, the differential adhesion hypothesis (DAH) [16] proposed that cell types can have distinct adhesion properties. Subsequent experiments demonstrated that a surface tension-like quantity can be assigned to cohesive cell clusters and this quantity predicts the spatial arrangement of cell sorting experiments [38]. The biophysical mechanism behind the macroscopic surface tension can be traced back to the amount of adhesion molecules, primarily cadherins, on the cell surface [39, 40], and a spatially restricted force generation within the cortical cytoskeleton [41]. The clarity of the DAH made it well suited for theoretical models which assumed that changes in cell configuration are driven by minimization of a quantity analogous to surface energy. This insight led to the widespread use of the Cellular Potts Model (CPM) to describe dynamics of multicellular systems [42], or a variety of multi-particle models which represent intercellular

adhesion by a combination of short range repulsive and a somewhat longer range attractive forces [21, 43, 44].

While the fast ($z \approx 1$) segregation of cells has been demonstrated using three dimensional aggregates [17], similarly fast kinetics was indicated in recent (two dimensional) monolayer cell culture experiments as well [18]. Although the fast segregation in 3D could be a consequence of hydrodynamic effects [45] such as mechanical pressure created by the cells, the firm adhesion between the cells and the culture substrate in monolayer experiments [18] points to the importance of active cell movements in the process. In this work we demonstrated using a previously proposed SPP model for multicellular behavior that suitable steering of active motility can indeed result in fast segregation with a kinetics compatible with experimental observations. The model is biologically plausible in the sense that the steering rule does not assume the cells' ability to calculate the local average direction of motion – a common assumption in SPP models. Instead, the effect of adjacent cells is deduced indirectly through the (in)ability to move in certain directions.

Supplementary Material

Refer to Web version on PubMed Central for supplementary material.

Acknowledgments

Funds from the European Union ERC COLLMOT Project, from the Hungarian Science Fund (K72664), the Hungarian Development Agency (KTIA AIK 12-1-2012-0020) and from the NIH (R01HL087136) are gratefully acknowledged.

References

1. Vicsek T, Zafeiris A. Physics Reports. 2012; 517:71.
2. Kudrolli A, Lumay G, Volfson D, Tsimring LS. Physical Review Letters. 2008; 100:058001. [PubMed: 18352433]
3. Palacci J, Abécassis B, Cottin-Bizonne C, Ybert C, Bocquet L. Physical Review Letters. 2010; 104:138302. [PubMed: 20481918]
4. Buttinoni I, Bialké J, Kümmel F, Löwen H, Bechinger C, Speck T. Physical Review Letters. 2013; 110:238301. [PubMed: 25167534]
5. Ni R, Stuart MAC, Dijkstra M. Nature Communications. 2013; 4
6. Búzás A, Kelemen L, Mathesz A, Oroszi L, Vizsnyiczai G, Vicsek T, Ormos P. Applied Physics Letters. 2012; 101:041111.
7. Bricard A, Caussin JB, Desreumaux N, Dauchot O, Bartolo D. Nature. 2013; 503:95. [PubMed: 24201282]
8. Marchetti MC, Joanny JF, Ramaswamy S, Liverpool TB, Prost J, Rao M, Simha AR. Reviews of Modern Physics. 2013; 85:1143.
9. Kabla AJ. Journal of The Royal Society Interface. 2012; 7:3268.
10. McCandlish SR, Baskaran A, Hagan MF. Soft Matter. 2012; 8:2527.
11. Bray AJ. Advances in Physics. 2002; 51:481.
12. Nakajima A, Ishihara S. New Journal of Physics. 2011; 13:033035.
13. Cremer P, Löwen H. Physical Review E. 2014; 89:022307.
14. Silverberg JL, Bierbaum M, Sethna JP, Cohen I. Physical Review Letters. 2013; 110:228701. [PubMed: 23767754]
15. Méhes E, Vicsek T. Integrative Biology. 2014; 6:831–854. [PubMed: 25056221]

16. Steinberg MS. Science. 1963; 141:401. [PubMed: 13983728]
17. Beysens DA, Forgács G, Glazier JA. Proceedings of the National Academy of Sciences of the USA. 2000; 97:9467. [PubMed: 10944216]
18. Méhes E, Mones E, Németh V, Vicsek T. PLoS ONE. 2012; 7:e31711. [PubMed: 22359617]
19. Stenhammar J, Tiribocchi A, Allen RJ, Marenduzzo D, Cates ME. Physical Review Letters. 2013; 111:145702. [PubMed: 24138255]
20. Belmonte JM, Thomas GL, Brunnet LG, de Almeida RMC, Chaté H. Physical Review Letters. 2008; 100:248702. [PubMed: 18643634]
21. Szabó B, Szöllősi GJ, Gönci B, Jurányi Z, Selmeczi D, Vicsek T. Physical Review E. 2006; 74:061908.
22. Akansu AN, Serdijn WA, Selesnick IW. Physical Communication. 2010; 3:1–18.
23. Verkhovsky AB, Svitkina TM, Borisy GG. Curr Biol. 1999; 9:11. [PubMed: 9889119]
24. Yam PT, Wilson CA, Ji L, Hebert B, Barnhart EL, Dye NA, Wiseman PW, Danuser G, Theriot JA. J Cell Biol. 2007; 178:1207. [PubMed: 17893245]
25. Kozlov MM, Mogilner A. Biophys J. 2007; 93:3811. [PubMed: 17704154]
26. Tambe DT, Hardin CC, Angelini TE, Rajendran K, Park CY, Serra-Picamal X, Zhou EH, Zaman MH, Butler JP, Weitz DA, et al. Nat Mater. 2011; 10:469. [PubMed: 21602808]
27. Weber GF, Bjerke MA, DeSimone DW. Dev Cell. 2012; 22:104. [PubMed: 22169071]
28. Dawes AT, Edelstein-Keshet L. Biophys J. 2007; 92:744. [PubMed: 17098793]
29. Szabó A, Ünnep R, Méhes E, Twal WO, Argraves WS, Cao Y, Czirók A. Phys Biol. 2010; 7:046007. [PubMed: 21076204]
30. Vicsek T, Czirók A, Ben-Jacob E, Cohen I, Shochet O. Physical Review Letters. 1995; 75:1226–1229. [PubMed: 10060237]
31. Henkes S, Fily Y, Marchetti MC. Physical Review E. 2011; 84:040301.
32. Peruani F, Klauss T, Deutsch A, Voss-Boehme A. Physical Review Letters. 2011; 106:128101. [PubMed: 21517352]
33. Redner GS, Hagan MF, Baskaran A. Physical Review Letters. 2013; 110:055701. [PubMed: 23414035]
34. Fily Y, Marchetti MC. Physical Review Letters. 2012; 108:235702. [PubMed: 23003972]
35. Peruani F, Deutsch A, Bär M. Physical Review E. 2006; 74:030904.
36. Ginelli F, Peruani F, Bär M, Chaté H. Physical Review Letters. 2010; 104:184502. [PubMed: 20482178]
37. Peruani F, Starruss J, Jakovljevic V, Søgaard-Andersen L, Deutsch A, Bär M. Physical Review Letters. 2012; 108:098102. [PubMed: 22463670]
38. Foty RA, Pfleger CM, Forgacs G, Steinberg MS. Development. 1996; 122:1611. [PubMed: 8625847]
39. Foty RA, Steinberg MS. Dev Biol. 2005; 278:255. [PubMed: 15649477]
40. Hegedűs B, Marga F, Jakab K, Sharpe-Timms KL, Forgacs G. Biophysical Journal. 2006; 91:2708. [PubMed: 16829558]
41. Maître JL, Berthoumieux H, Gabriel SF, Salbreux G, Jülicher F, Paluch E, Heisenberg CP. Science. 1012; 338:253. [PubMed: 22923438]
42. Glazier JA, Graner F. Physical Review E. 1993; 47:2128.
43. Newman T. Math Biosci Eng. 2005; 2:611.
44. Szabo A, Perryn ED, Czirok A. Physical Review Letters. 2007; 98:038102. [PubMed: 17358734]
45. Siggia ED. Physical Review A. 1979; 20:595.

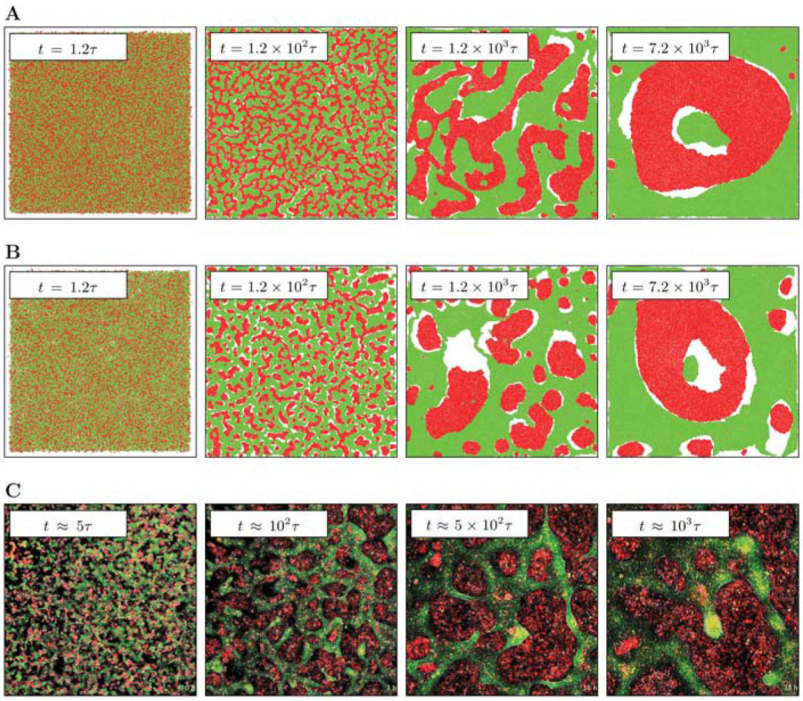

FIG. 1.

Morphologies characterizing the segregation of a SPP mixture at 50:50 (a) and at red:green = 40:60 (b) coverage ratios. Red particles are more motile than green particles (see Table I, $N = 10^5$, $L = L_0 = 100$). White areas are devoid of particles – uniform clusters can achieve higher local cell density than areas where the two particle types are intermixed and their movement is less correlated. In the final state of the simulation the red cluster rotates (see supplemental material). As a comparison, we show characteristic images from the experiment of [18] (c). Time unit t corresponds to the time needed for an SPP particle or cell to move a distance that is equal to the average particle/cell size.

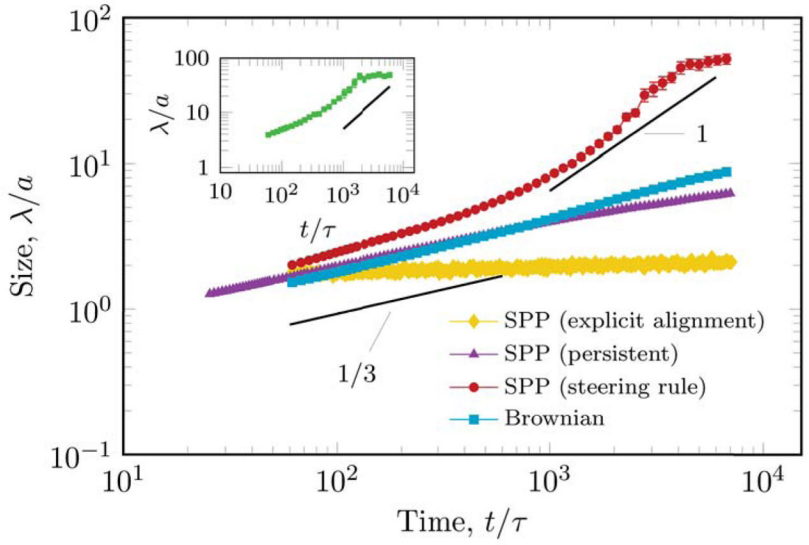

FIG. 2.

An SPP system can segregate much faster than a similar system containing noise-driven (Brownian) particles. In Brownian simulations the characteristic linear size of the segregated domains grows according to the Cahn-Hilliard behavior. In contrast, the SPP system with steering rule (7) exhibits a regime where the average cluster size is proportional to time. Fast segregation is also observed in simulations where all particles have identical properties (values characterizing red particles in Table I), and the segregation is driven only by the lack of adhesion between red and green particles (inset, noise=6.3°, coverage: 70%). Persistent random motility without the specific steering rule (7) also exhibits Cahn-Hilliard coarsening. The solid lines are guides to the eye. Spatial scale unit is the mean particle diameter, temporal unit is the time an SPP needs to move a unit distance. Error bars represent standard error of the mean ($\leq n \leq 12$).

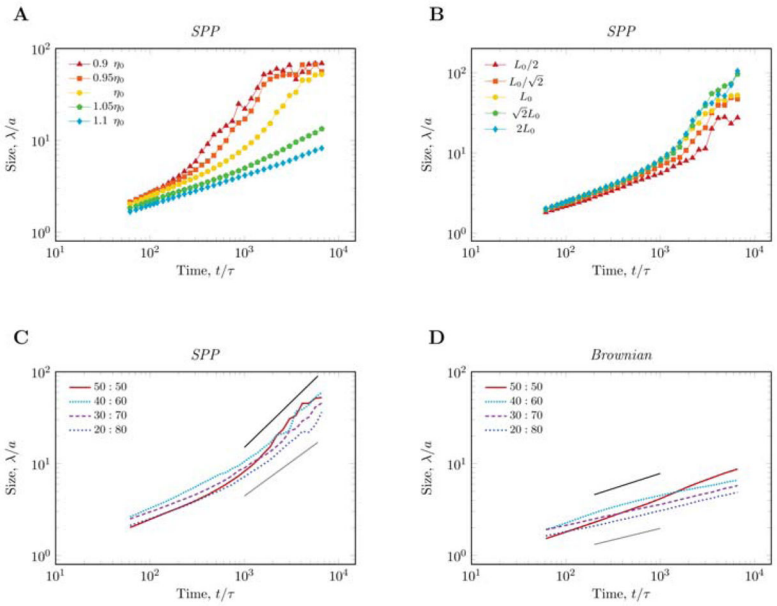

FIG. 3.

Cluster size dynamics for various model parameter values. A: Better steering quality (decreased noise) yields earlier and faster segregation. The transition between the fast ($z \approx 1$) and slow ($z \approx 1/3$) mechanism is sudden (elicited by a 10% change in the noise parameter) and is coincident with the transition between a long-range ordered (rotating) and a locally ordered, but globally disordered system. In the transient regime (red symbols) the velocity correlation length is still smaller than the system size, yet the segregation is much faster than the Cahn-Hilliard behavior. B: Maximal cluster size is limited by the system size. For larger systems the linear growth regime is extended. C: When the coverage ratio differs from 1:1, the segregation is slower than the linear growth shown in panels A and B, yet it is still faster than the Cahn-Hilliard behavior. D: As a comparison, noise driven particle system exhibit Cahn-Hilliard segregation with $z \approx 1/3$ for 1:1 coverage ratio and $z \approx 1/4$ otherwise.

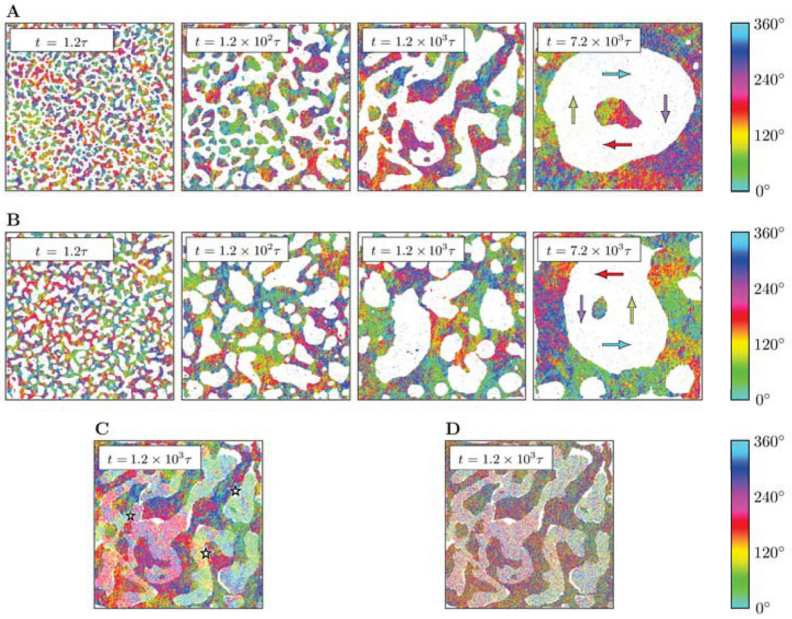

FIG. 4.

Directions of particle movements at various stages of the segregation process. Panels (A) and (B) depict color coded velocity directions of one particle type, the green particles, shown in Fig 1 at 50:50 (A) and red:green = 40:60 (B) coverage ratios. C: Velocity directions of both red and green particles within the system shown in panel A. The abrupt change of motion direction at segregation boundaries (asterisks) indicates that segregated cell groups can slide against each other. D: Heading directions in the same snapshot shown in panel C. Gray colors indicate that heading directions are less correlated locally than actual displacements are.

TABLE I

The set of parameters appearing in Eqs. (3)–(7), along with their corresponding symbols and simulational values.

Parameter description	Name	Value
red cell velocity	$v_{\mathcal{R}}$	3.125
green cell velocity	$v_{\mathcal{G}}$	1.25
repulsive force coeff.	F_{rep}	187.5
red-red adhesive force coeff.	$F_{adh}^{\mathcal{R}-\mathcal{R}}$	30
green-green adhesive force coeff.	$F_{adh}^{\mathcal{G}-\mathcal{G}}$	7.5
noise	$\eta_0\sqrt{\Delta t}$	7° in degrees

TABLE II

Power-law exponents in the different models (SPP and Brownian), with even and uneven (red:green = 40:60) volume fractions. The values correspond to the averages of fits to 4 trends, where each trend is averaged over 3 independent measurement. Errors idicate the standard deviations.

Dynamics	Exponent
SPP (50:50)	1.14 ± 0.12
SPP (40:60)	0.75 ± 0.05
Brownian (50:50)	0.38 ± 0.02
Brownian (40:60)	0.24 ± 0.02